Korean J. Chem. Eng., **26**(2), 554-559 (2009)

Kinetic analysis of NO-Char reaction

Shaozeng Sun, Juwei Zhang†, Xidong Hu, Penghua Qiu, Juan Qian, and Yukun Qin

Combusting Engineering Research Institute, School of Energy Science and Engineering, Harbin Institute of Technology, 92, West Dazhi Street, Harbin 150001, P. R. China
(*Received 19 July 2008 • accepted 15 October 2008*)

Abstract−Two Chinese coals were used to prepare chars in a flat flame flow reactor which can simulate the temperature and gas composition of a real pulverized coal combustion environment. Acid treatment on the YB and SH chars was applied to obtain demineralized chars. Kinetic characterization of NO-char reaction was performed by isothermal thermogravimetry in the temperature range of 973-1,573 K. Presence of catalytic metal matter can increase the reactivity of chars with NO, which indicates that the catalytic effects of inherent mineral matter play a significant role in the NO-char reaction. The discrete random pore model was applied to describe the NO-char reactions and obtain the intrinsic kinetics. The model can predict the data for all the chars at various temperatures well, but underestimate the reaction rates at high carbon conversions for the raw YB and SH chars, which can be attributed to the accumulation of metal catalyst on char surface.

Key words: Char, NO, Reducing Condition, Kinetics, Pore Model

INTRODUCTION

The reaction of nitrogen monoxide with char is of special interest due to its importance in producing or reducing NO emission from combustion system such as fluidized bed or pulverized coal combustion boiler [1-7]. Most published studies focused on common temperatures in fluidized bed, which are between 873 and 1,273 K [8-11]. Only few studies have been done at high temperature above 1,473 K, which is relevant to pulverized coal combustion. Song et al. [12] studied the NO-char reaction in a flow reactor in the temperature range 1,250-1,750 K and reached the conclusion that the order of reaction is unity with respect to NO. Levy et al. [13] measured the reaction rate in the temperature range 1,250-1,750 K and concluded that the NO-char reaction is slightly sensitive to variations in the gas composition, with the presence of carbon monoxide enhancing the reaction, whereas water has an inhibitory effect. Schonenbeck at al. [14] studied the heterogeneous reaction between NO and a coal-char in the temperature range 1,273-1,573 K in a drop tube furnace. The results support the assumption of first-order reaction with respect to NO concentration and surface area of char, and the activation energy is determined by combination of experiment and CFD simulation.

Despite extensive literature about the reduction of nitrogen monoxide by char, the mechanism of the reaction is still not clearly understood, and there are large variations in the data of reaction [15]. These variations can be attributed to the existence of many factors, such as parent coal rank, the catalytic inherent mineral matter, mass transfer limitations at higher temperatures and the effects of other gases etc.

The NO-char reaction is described by the following overall reaction:

$$2NO+C \rightarrow N_2+CO_2 \quad (1)$$

$$NO+C \rightarrow 1/2N_2+CO \quad (2)$$

Generally, the CO/CO_2 ratio has been observed to increase monotonically with temperature [11,15]; therefore, it is easy to speculate that reaction (2) will be the main reaction at high temperature.

The specific reaction rate of a gas-solid reaction can be defined as:

$$R = \frac{1}{1-X}\frac{dX}{dt} \quad (3)$$

where X is carbon conversion defined by:

$$X = \frac{m_0 - m_t}{m_0 - m_a} \quad (4)$$

At constant temperature, under kinetic control, the rate is a function of the concentration of reactants. Assuming first-order dependence on carbon concentration and pseudo-zero-order dependence on gas concentration (constant partial pressure of the reactant gas or excess gas), the specific reaction rate can be written as:

$$R = \frac{1}{1-X}\frac{dX}{dt} = kC_C \quad (5)$$

In general, the carbon active sites concentration can be written as a function of carbon conversion [9,16,17], i.e., C_C=f(X). And this functional relationship is the key to the determination of fundamental rate constants.

In this study, the coal char was prepared in a flat flame flow reactor (FFR) that can simulate the temperature and gas-phase environment in the near burner zone (flame region) of an industrial pulverized coal-fired furnace. The isothermal kinetic experiment was performed in a thermogravimetric analyzer (TGA). The purpose of this study was to explore the kinetics of the NO-char

†To whom correspondence should be addressed.
E-mail: zhangjw@hit.edu.cn
‡This work was presented at the 7th China-Korea Workshop on Clean Energy Technology held at Taiyuan, Shanxi, China, June 26-28, 2008.

reaction in a wide temperature range of 973-1,573 K.

EXPERIMENT

1. Sample Preparation

Two Chinese coals, a lignite (YB) and a bituminous (SH) coal, were used. The raw coals were sieved to obtain the 53-75 μm size fraction. The chars were prepared from the coals in an FFR. The FFR uses the hot products of the $CH_4/CO/O_2/N_2$ combustion flame to heat the char particles, thus closely approximating the temperature and gas composition of real pulverized coal combustion environment [18]. Coal particles were pyrolyzed in the post-flame zone of the flat flame operated under fuel rich conditions (equivalence ratio ϕ=1.4) with almost no oxygen existing in the region, so that this experiment may be more representative of the fuel-rich region in a coal flame than experiments conducted in inert gases such as nitrogen or argon [18,19].

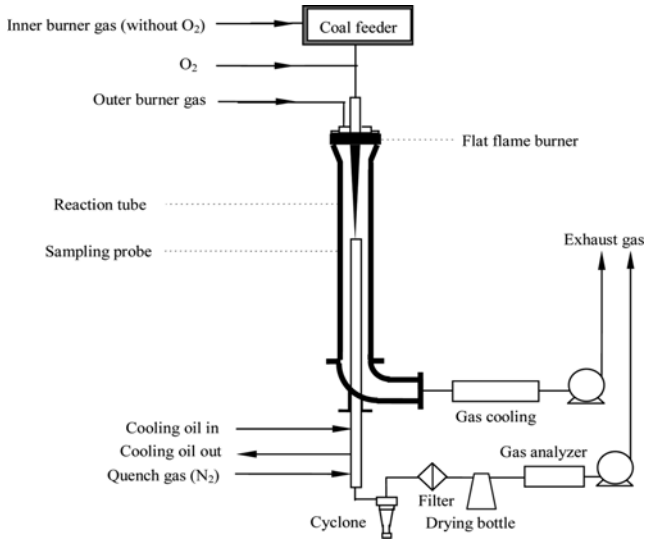

Fig. 1. Schematic of FFR facility.

A schematic of the FFR system is shown in Fig. 1. The key part of the system is a McKenna flat flame burner, which is modified from a standard McKenna burner. An inner burner was added to the standard burner in order to introduce particles. The inner burner was operated with the same equivalence ratio as the outer burner. Maximum particle heating rate in the FFR was 10^5 K/s. The flame temperature and post-flame gas component were calculated by using CHEMKIN4.0 on the assumption that the reactions could achieve equilibrium. In fact, the major species concentrations were very close to chemical equilibrium [20]. The calculated results are displayed in Table 1.

Coal particles were fed into the inner burner with a particle feeder and the feeding rate was 2 g/h. This feeding rate minimized the interaction of particles and permitted single particle reaction behavior. The inner burner gases (without O_2) were used to entrain coal particles. The gas flow was regulated by mass flow controllers. The particle collection system includes an oil-cooled, nitrogen-quenched probe followed by gas-solid separating devices. Residence time can be changed by raising or lowering the probe and the particle residence time in this experiment was around 40 ms.

To examine the catalytic effect of inherent mineral matter on char reactivity, the chars were washed by HCl and HF to remove essentially almost all the inorganic constituents. The demineralization procedure was originally developed by Harold [21]; the detailed process is as follows: 5 g of char was treated with 50 ml concentrated

Table 1. Results of CHEMKIN equilibrium calculation

Adiabatic flame temperature (K)	Gas composition after combustion (vol%)			
T	N_2	CO_2	H_2O	CO
2004	72.87	13.03	9.8	9.83

Table 2. Properties of coals and chars

Property	YB-coal	YB-char	DMYB-char	SH-coal	SH-char	DMSH-char
Proximate analysis (db)						
Fixed carbon	44.7	62.3	84.6	59.4	80.8	88.1
Volatile matter	36.2	5.4	10.8	29.4	3.8	9.8
Ash	19.1	32.3	4.6	11.2	15.4	2.1
Ultimate analysis (daf)						
C	73.1	83.2	96.5	76.1	90.8	92.6
H	5.7	1.4	1.0	4.6	1.2	0.6
N	1.0	1.2	0.9	1.4	1.0	0.9
Ash analysis (%)						
CaO	7.03	-	-	21.26	-	-
MgO	1.27	-	-	0.95	-	-
Na_2O	2.3	-	-	2.99	-	-
K_2O	2.28	-	-	1.96	-	-
TiO_2	0.48	-	-	0.37	-	-
Fe_2O_3	13.31	-	-	22.52	-	-
Surface area (m^2g^{-1})[a]	-	292	311	-	134	120

[a]Calculated on dry ash-free basis

HCl for 1 h at 50 ºC, filtered and washed, then treated with 50 ml concentrated HF under the same conditions, and finally the concentrated HCl acid treatment was repeated. The demineralized chars were washed with deionized water until no silver chloride was detected upon addition of silver nitrate solution to the filtrate. The analyses of raw coal/char and demineralized char are listed in Table 2. The ash content of chars was not measured, since the amounts of samples in this study were too small to be measured. However, the acid treatment in this study can remove essentially all the inorganic constituents [16].

2. Char Reactivity Measurements

Reactivity measurements of the chars were carried out in a TGA (Mettler-Toledo TGA/SDTA851^e) by isothermal analysis. Argon (99.999% purity) was used as the purge and balance gas. About 1 mg of char was placed in an alumina pan. The gas flow rate was maintained at 250 ml/min and the NO concentration was 1% (v/v). The sample was degassed at 323 K for 80 min before the experiment. After degassing, the temperature was raised to reaction temperatures ranging from 973 to 1,573 K; then the mixture of demanded NO concentration was introduced to the furnace. The weight changing details were recorded continuously as a function of time. Preliminary runs were carried out to determine the values of sample mass and gas flow rate to eliminate bulk diffusion limitations. Some repeat experiments were conducted to confirm the reliability of the data obtained in this study. And the measured results are very stable due to the excellent performance of TGA used in this study.

3. Char Characterization Measurements

The gas adsorption method was applied to analyze the pore structure of chars. An automated adsorption analyzer AUTOSORB-1-C (Quanta Chrome Corp.) was used. The adsorption/desorption isotherms were obtained with nitrogen at 77.4 K in a relative pressure between 0.01 and 0.978. The specific surface area and mesopore size distributions were calculated by the BET-equation and BJH method, respectively. The results are given in Table 2.

RESULTS AND DISCUSSION

1. Char Reactivity at Various Temperatures

According to the unification approach proposed by Mahajan et al. [22], under different temperatures, pressures, gasification agents and chars, char gasification curves in the form of carbon conversion X versus gasification time t can be approximately unified into a single curve when X is plotted against the dimensionless times τ, where $\tau=t/t_{1/2}$, $t_{1/2}$ being the half-life of the char-gas reaction. Kasaoka et al. [23] proposed the expression as follows:

$$X=1-\exp(-A\tau^B) \quad (6)$$

The master curve in Fig. 2 is obtained according to the expression above which can unify the experimental data well. In Fig. 2, DMYB and DMSH denote demineralized YB and SH char. However, the scatter of data increases when X>0.7, which was also found by Kasaola et al. [23] and Raghunathan et al. [24].

Fig. 3 shows the Arrhenius plots of two chars and their demineralized chars at a given carbon conversion level. A good linear relationship can be obtained for all cases. It is observed that there are two temperature regimes of activation energy (i.e., the slopes of lines) for all the cases. The transition temperatures T_t for raw chars and demineralized chars are around 1,173 K and 1,273 K, respectively. In fact, the precise values of T_t are not what we are concerned about. However, it is important that the activation energies obtained below T_t are obviously higher than that obtained above T_t. And the variations of activation energies indicate that the reactions were under chemical kinetic control in the low-temperature regime (below T_t) and under diffusion control in the high-tempera-

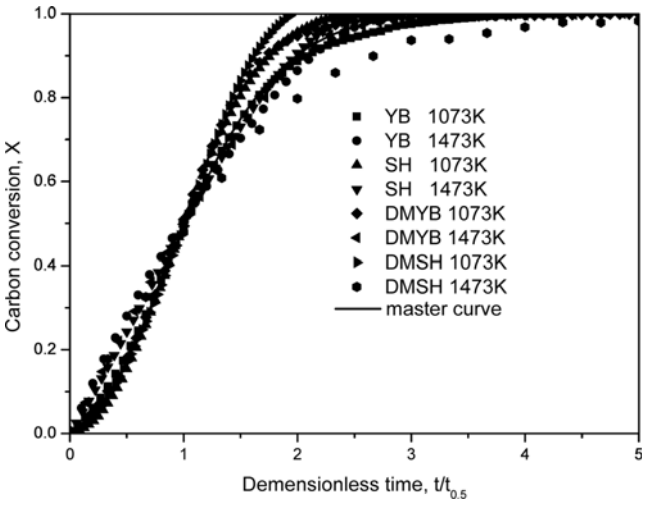

Fig. 2. Unification of experimental carbon conversion data for different chars and temperatures.

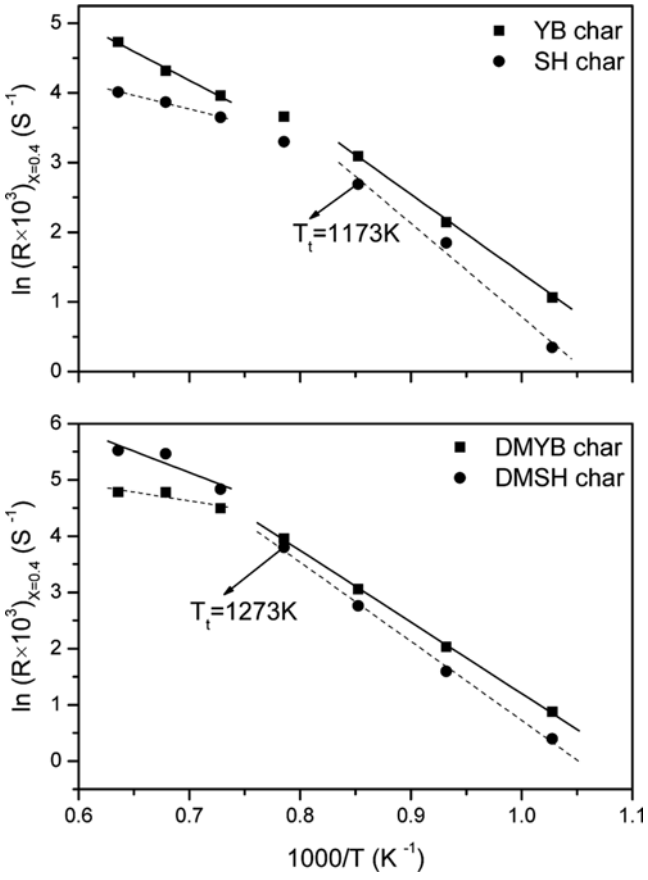

Fig. 3. Arrhenius plots of NO-char reaction.

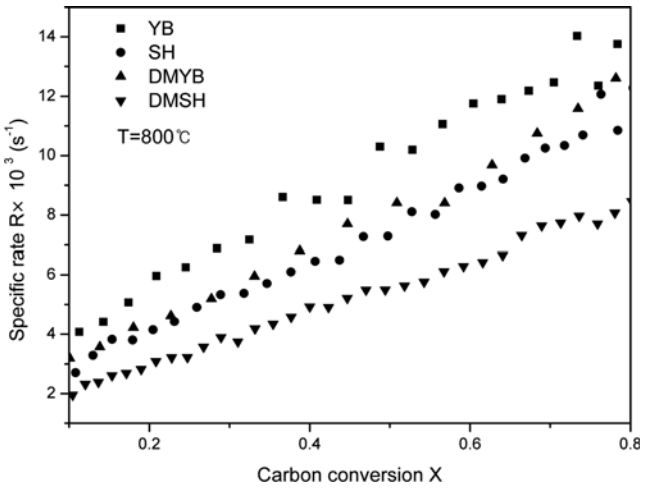

Fig. 4. NO-char specific rate versus carbon conversion.

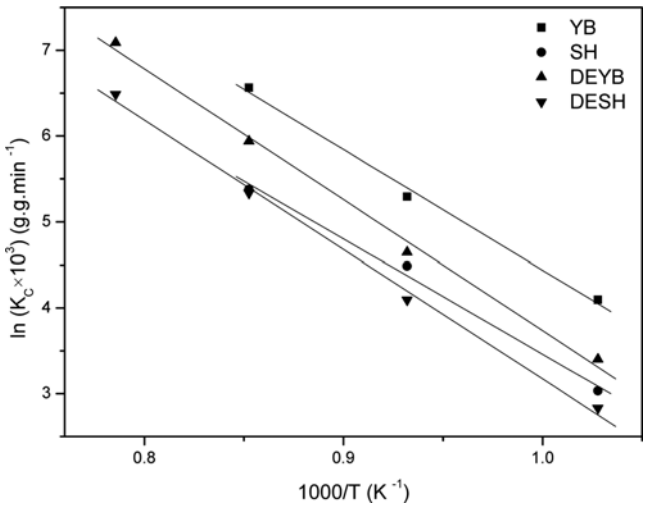

Fig. 5. Arrhenius plots of NO-char reaction from the discrete random pore model.

ture regime (above T_t).

Fig. 4 shows the specific reaction rate versus carbon conversion curves at a given temperature for all chars. A monotonically increasing rate is observed in all cases. This is similar to the other char gasification behaviors [9,20,25]. The reactivity of YB char is obviously higher than SH char, which can be attributed to larger surface area (see Table 2) and lower carbon content for YB char [26]. However, it can be seen that the reactivity of chars is not proportional to the nitrogen BET surface area, and previous studies revealed that there were better correlations between the NO reduction rate and the micropore area (obtained by CO_2 adsorption) or the macropore area (obtained by mercury porosimetry) [9,27].

According to Fig. 4, the demineralization evidently decreases the reactivity of both chars. Reactivity of both chars is strongly influenced by demineralization due to the decrease of inherent catalytic mineral content during the acid treatment. Therefore, the catalytic effects of inherent mineral matter play a significant role in the NO-char reaction, which has been presented by Aarna et al. [15], Illan-Gomez et al. [28] and Salvador et al. [29]. The YB and SH coal are both rich in catalytic metals such as Fe, Ca, Na, K, Mg, Ti (see Table 2), so the catalytic effects of metals cannot be ignored.

2. Pore Structure Model Analysis

To quantitatively interpret the experimental data in the kinetic control regime, the random pore model (RPM) developed by Bhatia and Perlmutter [30] was applied. This model accounts for the overlapping of reacting surfaces as they grow, and has shown its wide applicability in the prediction of char reaction rate versus conversion [31,32]. Since the chars in this study were microporous, the discrete random pore model (DRPM) [33] was used to explain the experimental data. Compared with original RPM, DRPM accounts for the discreteness of the solid phase. The original DRPM assumed that the reaction is under kinetic control, and the total surface area TSA as a function of carbon conversion X is expressed by:

$$\mathrm{TSA} = \mathrm{TSA}_0\sqrt{1-\psi_E \ln(1-\mathrm{X})} \tag{7}$$

Where ψ_E is a structure parameter defined as follows:

$$\psi_E = \frac{4\pi L_{EO}(1-\varepsilon_0)^2}{\mathrm{TSA}_0^2(1+\alpha)^2} \tag{8}$$

Assuming that the reaction occurs on the entire surface, i.e., C_C= TSA, according to (3):

$$\mathrm{R} = k_S \mathrm{TSA}_0\sqrt{1-\psi_E \ln(1-\mathrm{X})} = k_C\sqrt{1-\psi_E \ln(1-\mathrm{X})} \tag{9}$$

The rate constant k_C and pore structure parameter ψ_E can be obtained by fitting the experimental data at various temperatures to (9). In this study, in order to obtain intrinsic kinetic parameters, only the data in low-temperature regime were used. The results are shown in Table 3. According to the Arrhenius equation, the activation energies and pre-exponential factors were obtained from the k_C, and

Table 3. Kinetic parameters from the discrete random pore model

Reaction temperature (K)	YB char		DMYB char		SH char		DMSH char	
	$k_C\times10^3$ (g g^{-1} s^{-1})	ψ_E	$k_C\times10^3$ (g g^{-1} s^{-1})	ψ_E	$k_C\times10^3$ (g g^{-1} s^{-1})	ψ_E	$k_C\times10^3$ (g g^{-1} s^{-1})	ψ_E
973	1	10	0.5	24	0.35	36.01	0.28	37.5
1,073	3.32	9.09	1.73	24	1.48	35.45	1	38
1,173	11.83	4.3	6.32	17.5	3.61	31.38	3.46	41.67
1,273	-		20	12.5	-	-	10.95	30
Activation energy (kJ/mol)	116.4		126.9		111.7		125.4	
Pre-exponential factor (g g^{-1} s^{-1})	14.39		14.90		12.80		14.16	

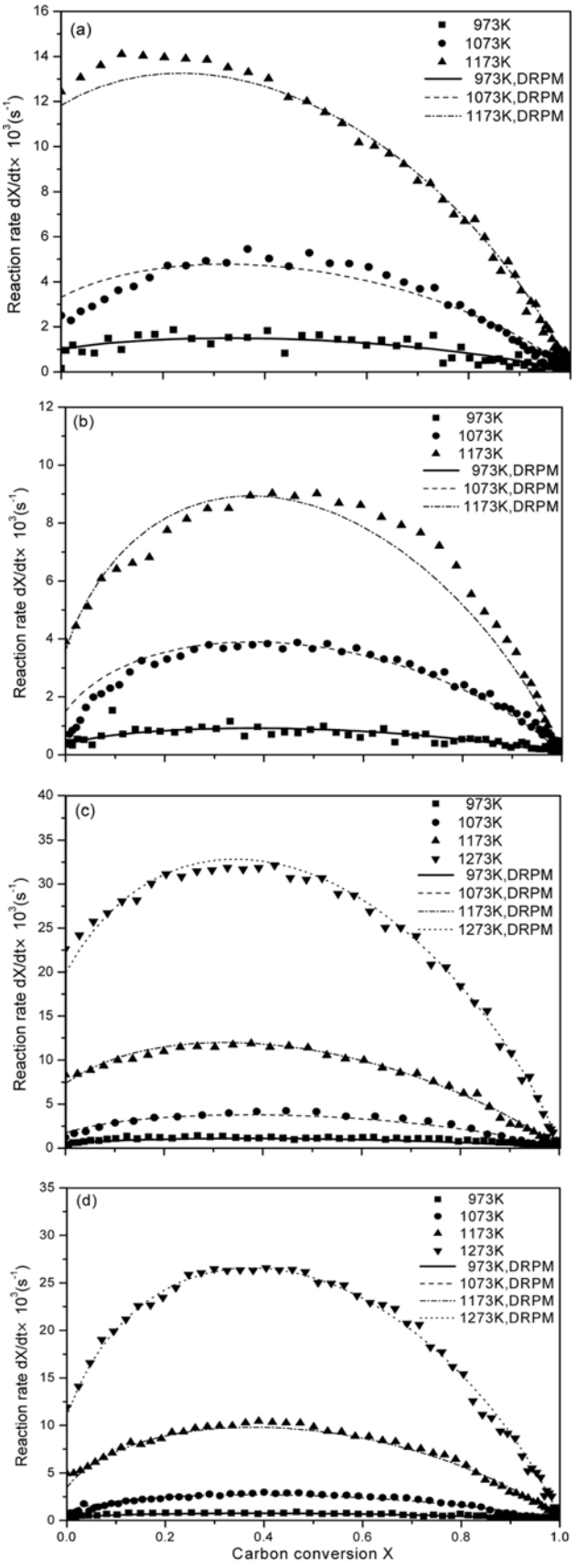

Fig. 6. Experimental and fitted reaction rates as a function of carbon conversion: (a) YB char; (b) SH char; (c) DMYB char; (d) DMSH char.

the Arrhenius plots for both chars are shown in Fig. 5. The good linear relationship obtained for all chars confirms that the reactions of chars in the low-temperature regime were under chemical kinetic control. From Table 3, it can be seen that reactions of demineralized chars have higher activation energies than those of parent chars. This indicates that the presence of catalytic metal matter can decrease the apparent activation energy of the reaction. The presence of catalytic metal matter catalyzes the NO-carbon reaction both by increasing the number of active sites and/or the turnover rate on these sites as well as by significantly decreasing the activation energy [11]. The obtained activation energies (126.9 and 125.4 kJ/mol) are in good agreement with other data presented in literature [9,14,15]. This indicates that as a simple and rapid method, TGA can be an available tool to characterize the kinetics of the NO-char reaction.

In Fig. 6, the experimental results of reaction rates versus carbon conversion are compared with the predictions by the DRPM. For all the chars, the predicted curve is in good agreement with that of the experimental data at different temperatures. For the raw YB and SH chars, the DRPM underestimates the experimental results at high carbon conversions, and the maximum reaction rate is shifted towards higher conversions. This can be attributed to the catalytic effects of inherent minerals in chars. According to mathematical analysis of RPM by Bhatia and Perlmutter [30], the position of the maximum rate should be restricted to the range $0 \le X \le 0.393$. However, previous studies [34-36] have revealed that the peak rate can be shifted towards higher conversions due to the accumulation of metal catalyst on the char surface. The ash of the YB and SH chars are both rich in catalytic metals. These catalytic metals can enlarge the number of active sites on carbon surface and decrease the activation energy without fundamentally changing the kinetic mechanism [28,37].

CONCLUSION

Char samples were obtained from two Chinese low-rank coals in an FFR which can simulate a true pulverized coal combustion environment. The kinetics of NO-char reaction was studied in a thermogravimetric analyzer in the temperature range of 973-1,573 K.

Experimental data for all the chars can be unified into a single master curve, carbon conversion versus dimensionless time.

The NO-char reactions were under chemical kinetic control in the low-temperature regime (below a transtion temperature T_t) for all the chars, and diffusional effects prevail for higher temperatures.

The YB char was proven to be more reactive, compared with the SH char due to its larger surface area and lower carbon content. The experimental data of demineralized chars reveal that the catalytic effects of inherent mineral matter play a significant role in the NO-char reaction. The presence of catalytic metal matter increases the reactivity and decreases the activation energies of chars with NO, and the accumulation of metal catalyst on char surface changes the shape of reaction rate curve.

The discrete random pore model can be used to describe the reaction of all chars satisfactorily, but it underestimates the reaction rates at high carbon conversions for the raw YB and SH chars, which can be attributed to the accumulation of metal catalyst on char surface. The determined intrinsic activation energies for two demineralized chars are 126.9 and 125.4 kJ/mol, which agrees satisfactorily

with those data in other literature.

ACKNOWLEDGMENTS

This work is sponsored by the Ministry of Science and Technology of China through the National Basic Research Program of China (contract No: 2006CB200303), the National High Technology Research and Development of China (contract No: 2007AA05Z336), Natural Science Foundation of China (contract No: 50576020), and the program of excellent Team in Harbin Institute of Technology.

NOMENCLATURE

X : carbon conversion [dimensionless]
m_0 : initial mass of char [g]
m_t : mass of char at time t [g]
m_a : mass of ash residue at the end of reaction [g]
K : rate constant [g g^{-1} s^{-1}]
C_C : concentration of carbon active sites [$g_{active\ carbon\ site}$·g^{-1}_{carbon}] which is conventionally identified with the total surface area (TSA) or the reactive surface area (RSA)
τ : dimensionless time τ, where $\tau=t/t_{1/2}$, $t_{1/2}$ being the half-life of the char-gas reaction [dimensionless]
TSA : total surface area per unit volume or gram of carbon at conversion X [m^{-1} or m^2 g^{-1}]
TSA_0 : initial surface area per unit volume or gram of carbon [m^{-1} or m^2 g^{-1}]
ψ_E : pore structure parameter [dimensionless]
L_{EO} : total initial length of the pore axes per unit volume [m^{-2}]
ε_0 : initial porosity [dimensionless]
α : discreteness parameter [dimensionless]
k_S : surface reaction rate constant [g m^{-2} s^{-1}]
k_C : rate constant independent of surface area [g g^{-1} s^{-1}]
C : mass fraction of carbon in coal as dry ash-free basis [%]
H : mass fraction of hydrogen in coal as dry ash-free basis [%]
N : mass fraction of nitrogen in coal as dry ash-free basis [%]

REFERENCES

1. M. Kang, J. H. Park, J. S. Choi, E. D. Park and J. E. Yie, *Korean J. Chem. Eng.*, **24**, 191 (2007).
2. P. H. Qiu, S. H. Wu, S. Z. Sun, H. Liu, L. B. Yang and G. Z. Wang, *Korean J. Chem. Eng.*, **24**, 683 (2007).
3. T. J. Li, Y. Q. Zhuo, J. Y. Lei and X. C. Xu, *Korean J. Chem. Eng.*, **24**, 1113 (2007).
4. Y. Zhang, Y. J. Ding, Z. S. Wu, L. Kong and T. Chou, *Korean J. Chem. Eng.*, **24**, 1118 (2007).
5. Z. Q. Li, Z. C. Chen, R. Sun and S. H. Wu, *J. Energy Institute*, **80**, 123 (2007).
6. Z. Q. Li, J. P. Jing, Z. C. Chen, F. Ren, B. Xu, H. D. Wei and Z. H. Ge, *Combust. Sci. Technol.*, **180**, 1370 (2008).
7. J. Cances, J. M. Commandre, S. Salvador and P. Dagaut, *Fuel*, **87**, 274 (2008).
8. H. Teng, E. M. Suuberg and J. M. Calo, *Energy & Fuels*, **6**, 398 (1992).
9. Y. H. Li, L. R. Radovic, G. Q. Lu and V. Rudolph, *Chem. Eng. Sci.*, **54**, 4125 (1999).
10. S. B. Wang, V. Slovak and B. S. Haynes, *Fuel Process Technol.*, **86**, 651 (2005).
11. D. Lopez and J. Calo, *Energy & Fuels*, **21**, 1872 (2007).
12. Y. H. Song, J. M. Beer and A. F. Sarofim, *Combust. Sci. Technol.*, **25**, 237 (1981).
13. J. M. Levy, L. K. Chan, A. F. Sarofim and J. M. Beer, *Eighteenth symposium (international) on combustion, the combustion institute*, 111 (1980).
14. C. Schonenbeck, R. Gadiou and D. Schwartz, *Fuel*, **83**, 443 (2004).
15. I. Aarna and E. M. Suuberg, *Fuel*, **76**, 475 (1997).
16. L. R. Radovic, P. L. Walker, Jr. and R. G. Jenkins, *Fuel*, **62**, 849 (1983).
17. A. A. Lizzio, H. Jiang and L. R. Liubisa, *Carbon*, **28**, 7 (1990).
18. D. Zeng, M. Clark, T. Gunderson, W. C. Hecker and T. H. Fletcher, *Proceedings of the combustion institute*, **30**, 2213 (2005).
19. T. H. Fletcher, J. L. Ma, J. R. Rigby, A. L. Brown and B. W. Webb, *Prog. Energy Combust. Sci.*, **23**, 293 (1997).
20. P. Weigand, R. Luckerath and W. Meier, Institute of Combustion Technology, www.dlr.de/VT/Datenarchiv.
21. H. D. Bale, M. L. Catlson and H. H. Schobert, *Fuel*, **65**, 1185 (1986).
22. O. P. Mahajan, R. Y. Yarzab and P. L. Walker, *Fuel*, **57**, 643 (1978).
23. S. Kasaoka, Y. Sakata and C. Tong, *Int. Chem. Eng.*, **25**, 160 (1985).
24. K. Raghunathan and R. Y. K. Yang, *Ind. Eng. Chem. Res.*, **28**, 518 (1989).
25. L. R. Radovic, H. Jiang and A. A. Lizzio, *Energy & Fuels*, **5**, 68 (1991).
26. S. H. Ng, D. P. Fung and S. Kim, *Fuel*, **67**, 700 (1988).
27. J. M. Commandre, B. R. Stanmore and S. Salvador, *Combustion and Flame*, **128**, 211 (2002).
28. M. J. Illan-Gomez, A. Linares-Solano, L. R. Radovic and D. L. C. Salinas-Martinez, *Energy & Fuels*, **10**, 158 (1996).
29. S. Salvador, J. M. Commandre, B. R. Stanmore and R. Gadiou, *Energy & Fuels*, **18**, 296 (2004).
30. S. K. Bhatia and D. D. Perlmutter, *AIChE J.*, **26**, 379 (1980).
31. J. L. Su and D. D. Perlmutter, *AIChE J.*, **31**, 973 (1985).
32. J. Ochoa, M. C. Casanello, P. R. Bonelli and A. L. Cukierman, *Fuel Process Technol.*, **74**, 161 (2001).
33. S. K. Bhatia and B. J. Vartak, *Carbon*, **34**, 1383 (1996).
34. R. Hamilton, T. Sams and D. A. Shadman, *Fuel*, **63**, 1043 (1984).
35. R. P. W. Strius, C. V. Scala, S. Stucki and R. Prins, *Chem. Eng. Sci.*, **57**, 3581 (2002).
36. R. P. W. Strius, C. V. Scala, S. Stucki and R. Prins, *Chem. Eng. Sci.*, **57**, 3593 (2002).
37. J. A. Moulijin and F. Kapteijin, *Carbon*, **33**, 1155 (1995).